



**HAL**  
open science

## behaviour in a N<sub>2</sub>NO surface dielectric barrier discharge in the modulated ac regime at atmospheric pressure

M Šimek, P F Ambrico, S de Benedictis, G Dilecce, V Prukner, J Schmidt

### ► To cite this version:

M Šimek, P F Ambrico, S de Benedictis, G Dilecce, V Prukner, et al.. behaviour in a N<sub>2</sub>NO surface dielectric barrier discharge in the modulated ac regime at atmospheric pressure. *Journal of Physics D: Applied Physics*, 2010, 43 (12), pp.124003. 10.1088/0022-3727/43/12/124003 . hal-00569556

**HAL Id: hal-00569556**

**<https://hal.science/hal-00569556>**

Submitted on 25 Feb 2011

**HAL** is a multi-disciplinary open access archive for the deposit and dissemination of scientific research documents, whether they are published or not. The documents may come from teaching and research institutions in France or abroad, or from public or private research centers.

L'archive ouverte pluridisciplinaire **HAL**, est destinée au dépôt et à la diffusion de documents scientifiques de niveau recherche, publiés ou non, émanant des établissements d'enseignement et de recherche français ou étrangers, des laboratoires publics ou privés.

# **$N_2(A^3\Sigma_u^+)$ behaviour in a $N_2$ –NO surface dielectric barrier discharge in the modulated AC regime at atmospheric pressure**

M Šimek<sup>1</sup>, P F Ambrico<sup>2</sup>, S De Benedictis<sup>2</sup>, G Dilecce<sup>2</sup>, V Prukner<sup>1</sup> and J Schmidt<sup>1</sup>

<sup>1</sup> Institute of Plasma Physics v.v.i., Department of Pulse Plasma Systems, Academy of Sciences of the Czech Republic, Za Slovankou 3, 182 00 Prague, Czech Republic

<sup>2</sup> Istituto di Metodologie Inorganiche e dei Plasmi - CNR, sede di Bari, via Orabona, 4, 70126 Bari, Italy

E-mail: [simek@ipp.cas.cz](mailto:simek@ipp.cas.cz)

**Abstract.** Optical, electrical and discharge product measurements were performed in order to reveal the behaviour of  $N_2(A^3\Sigma_u^+)$  metastables in a surface dielectric barrier discharge driven in  $N_2$  with small NO admixtures in a modulated AC regime. Metastable species were detected both in a thin surface plasma layer and in the space afterglow through Plasma Induced Emission and Optical-Optical Double Resonance Laser Induced Fluorescence, respectively. Basically, the observed  $N_2(A^3\Sigma_u^+)$  species follow the discharge current oscillations in the plasma layer, while they evolve on a millisecond time-scale due to diffusion through the space afterglow. Emission spectrometry provides a rough estimation of average metastable concentration in a thin surface plasma layer  $\sim 9 \times 10^{13} \text{ cm}^{-3}$ . Fluorescence measurements then allow an upper estimation of metastable concentration in the space afterglow  $\leq 1 \times 10^{12} \text{ cm}^{-3}$ .

Short title :  $N_2(A^3\Sigma_u^+)$  behaviour in surface DBD

## 1. Introduction

Atmospheric-pressure, non-equilibrium plasmas generated by surface dielectric barrier discharges (SDBDs) produce a highly reactive environment which is suitable for various applications, such as pollution control, sterilization, ozone generation or surface modification [1–4]. Generally, such discharges driven in nitrogen are characterised by substantial quantities of long-living (metastable) energy carriers (e.g.  $N_2(A^3\Sigma_u^+)$ ,  $N(^4S)$ ,  $N_2(X^1\Sigma_g^+, v>5)$ ) capable of affecting the physical chemistry of the discharge, however the production and relaxation of such species is still not fully explored [5].

Recently, several diagnostic approaches based on plasma induced emission (PIE) and laser induced fluorescence (LIF) techniques have been developed to quantify  $N_2(A^3\Sigma_u^+)$  species at atmospheric pressure [6–15]. While emission-based techniques [9–10] make use of elementary processes capable to link metastables with electronically-excited reference species that are readily observable in emission spectra [6,7], techniques based on LIF [12–15] utilize the interaction of external photons with the probed metastables. Nevertheless all former techniques have been applied to volume corona or DBD discharges. The first attempt to follow metastables produced in an AC continuously excited surface discharge has been reported in [13].

In this work, the behaviour of  $N_2(A^3\Sigma_u^+)$  metastables ( $N_2(A)$ ) produced by an atmospheric-pressure surface dielectric barrier discharge driven in the amplitude-modulated AC regime was investigated by combining PIE spectroscopy and optical-optical double resonance LIF (OODR-LIF) techniques. Joint experimental works reported here were performed partly at IPP Prague and partly at IMIP Bari. Investigations done at IPP Prague focused on electrical characteristics, PIE and discharge product measurements, while all OODR-LIF related experiments were realized at IMIP Bari. It is important to note, however, that both IPP and IMIP experimental data sets can be considered as fully complementary because all experiments were accomplished utilizing (i) the only portable compact SDBD reactor and (ii) equivalent high voltage AC power and gas feed supplies, as detailed in the following sections.

## 2. Experimental setup

The SDBD reactor designed at IPP Prague laboratories [16] consists of a planar electrode placed in a polyvinyl chloride (PVC) chamber equipped with gas feed input/output ports, a high voltage interface and three quartz windows suitable for PIE and OODR-LIF diagnostics. A block scheme of the experimental-up is shown in figure 1 and a simplified sketch of the SDBD reactor is shown in figure 2. The electrode system is made of a thin alumina plate (10 cm x 10 cm x 0.065 cm) with metallic electrodes deposited on both sides. The exposed discharge electrode consists of a set of parallel metallic strips (1 mm wide, 80 mm long and separated by 3 mm). A full square induction electrode covers the opposite surface of the alumina plate.

The SDBD reactor was powered at both sites by an AC power supply composed of a waveform generator, a wideband amplifier and a step-up transformer. Applied AC high voltage (5 kHz) was amplitude modulated (square-wave modulation waveform producing 5 kHz sine-wave ON/OFF periods with a variable duty cycle  $D = 0.048\text{--}0.33$  with  $T_{\text{ON}} = 1\text{--}10$  ms and fixed  $T_{\text{OFF}}=20$  ms). The voltage-charge/voltage-current discharge characteristics shown in the next section were recorded using a fast digitizing oscilloscope LeCroy WavePro7000 (bandwidth 1GHz, up to 10 GS/s). A Testec HVP 15HF high voltage probe was used to sample the discharge voltage waveforms. A Tektronix P6139A high voltage probe was used to measure the voltage drop on a non-inductive shunt resistor (current measurements) or on a measuring capacitor (charge measurements), both inserted alternately between the induction electrode and ground.

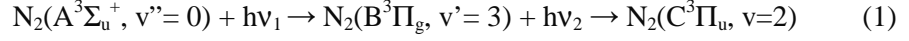
The discharge was fed either with pure nitrogen (standard 5.0 purity) or with  $\text{N}_2 + \text{NO}$  mixtures through mass-flow controllers (total flow  $\Phi = 1\text{--}10$  slm). To determine stable discharge products, quantified traces of NO were added through a controlled flux of  $\text{N}_2 + \text{NO}$  mixture (Pulmonix<sup>®</sup> forte, Messer Austria, 900 ppm NO in  $\text{N}_2$ , containing  $\text{H}_2\text{O} < 3$  ppm,  $\text{O}_2 < 1$  ppm and  $\text{NO}_2 < 1$  ppm as main impurities). An API 200EM chemiluminescence NO/ $\text{NO}_x$  analyzer and API 320E infrared  $\text{N}_2\text{O}$  analyzer (Teledyne Instruments) were used to quantify both initial mixture composition and stable discharge products.

The two small lateral windows shown in figure 2 were used to pass two collinear laser beams for OODR-LIF measurements, while a large frontal window was used to collect both PIE and OODR-LIF fluorescence signals perpendicularly to the discharge surface. Optical emission measurements were performed by means of a fast Hamamatsu R2949 photomultiplier (PMT) (always terminated by a 50  $\Omega$  load) which detected volume-averaged PIE waveforms collected through the quartz optical fibre bundle, lenses and interference filters. The PMT signal was sampled simultaneously by the oscilloscope and by a gated 200 MHz MSA-200 (Becker&Hickl) multichannel photon counter. Four interference filters were used to isolate specific emissions, namely:

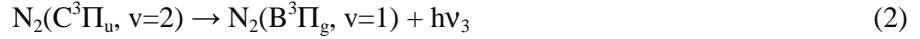
- (0,0) band of  $\text{N}_2^+(\text{B}^2\Sigma_u^+ \rightarrow \text{X}^2\Sigma_g^+)$  first negative system (1.NG) at 391 nm,

- (0,0) band of  $N_2(C^3\Pi_u \rightarrow B^3\Pi_g)$  second positive system (2.PG) at 337 nm,
- (2,0) band of  $N_2(C''^5\Pi_u \rightarrow A'^5\Sigma_g^+)$  Herman infrared system (HIR) at 710 nm,
- (0,2) band of  $NO(A^2\Sigma^+ \rightarrow X^2\Pi)$  system (NO- $\gamma$ ) at 257 nm.

The OODR-LIF technique employs resonant excitation of the  $N_2(A)$  metastable state to  $N_2(C^3\Pi_u)$  radiative state through an intermediate  $N_2(B^3\Pi_g)$  level by two synchronised photons tuned in this case to the following transitions [12–14].



The  $hv_1$  and  $hv_2$  photons were produced at  $\lambda_1 = 687$  nm ( $E_1 \sim 31$  mJ/pulse, typical pulse duration  $< 6$  ns) and at  $\lambda_2 = 350$  nm ( $E_2 \sim 1$  mJ/pulse, typical pulse duration  $< 9$  ns) by the two synchronised tuneable Nd-YAG pumped dye lasers. A master TTL trigger was used to modulate the discharge and to trigger the laser-delay cards generating a controlled delay with respect to the discharge modulation waveform. OODR-LIF fluorescence signal  $hv_3$  was then detected at  $\lambda_3 = 313.6$  nm through the 2.PG-(2,1) band.



The volume sampled by the OODR-LIF was imaged (1:1) onto the  $\sim 2 \times 2$  mm<sup>2</sup> entrance slit of the 0.5 m SPEX monochromator equipped with R2949 photomultiplier. Scattered laser photons were reduced by a notch filter centred at  $\lambda_1$  and combined with an interference filter transmitting the (2,1) band radiation, both placed in front of the SPEX entrance slit. Finally, the OODR-LIF signal was obtained after subtracting a contribution given by plasma induced emission from the total measured signal. The pure OODR-LIF signal then unambiguously monitors the evolution of  $N_2(A)$  in the space afterglow averaged over a cylindrical volume ( $h = 2$ mm,  $\phi = 1$ mm) centred at a fixed distance ( $\sim 1$  mm) from the discharge surface. All energy levels and transitions involved in monitoring  $N_2(A)$  species through PIE and OODR-LIF are schematically shown in figure 3.

### 3. Experimental results

When driving the discharge in the amplitude modulated AC regime at low duty cycle, a large number of nearly equally spaced micro-discharges cover the whole electrode surface as shown in figure 4. A small square in the middle of the figure indicates an area sampled by the OODR-LIF. In the case of PIE measurements, the sampled area was circular and roughly twice as large (diameter  $\sim 5$  mm). However, no luminous macro-streamers similar to those reported in the continuous AC regime [13] were observed (at least over the explored duty cycle range  $D = 0.048 - 0.33$ ), therefore the registered PIE signal is in this work definitely formed by averaging equivalent micro-discharges.

#### *Electrical characteristics and discharge products*

Voltage-charge/voltage-current SDBD characteristics were measured in order to define the discharge regime and the average power dissipated inside the plasma layer volume. Figure 5 shows a typical discharge voltage, the voltage drop on a measuring capacitor, the voltage drop on a non-inductive shunt resistor and a PMT signal for  $T_{ON} = 3$  ms. The voltage-charge (Lissajous) characteristics in figure 6 show typical hysteresis loops which are related to the amount of energy dissipated during a single AC cycle. It turns out that the energy dissipated during the first AC cycle is always larger than for the following cycles [16]. This is evidenced in figure 6 by a markedly larger area of the Lissajous plot obtained from the first AC cycle. Voltage-charge characteristics were therefore used to evaluate the energy dissipated during the  $T_{ON}$  period and the average discharge power. The energy dissipated during the  $T_{ON}$  period was found to be  $\sim 37$  mJ in pure nitrogen ( $T_{ON} = 3$  ms). For small NO admixtures of up to 20 ppm, we observed  $\sim 10$ -15% energy drop when maintaining a fixed HV AC amplitude. In both cases, the dissipated energy depends roughly linearly on  $T_{ON}$ .

Stable discharge products (NO/NO<sub>2</sub>/N<sub>2</sub>O) were monitored for both pure nitrogen (containing  $< 3$  ppm of O<sub>2</sub> as major impurity) and N<sub>2</sub>-NO mixture. Due to instrumental requirements (minimum gas flow rate), the dependence of the product composition on duty cycle was explored over a total gas flow range  $\Phi = 2.5 - 10$  slm. In the case of pure nitrogen, the only detectable product occurring at low duty cycle is N<sub>2</sub>O [16]. A reproducible level  $[N_2O]=0.35 \pm 0.02$  ppm was found for  $T_{ON} = 1$  ms and nitrogen flow  $\Phi = 5$  slm. With increasing  $T_{ON}$  we observed an N<sub>2</sub>O increase up to  $\sim 1.2$  ppm (for  $T_{ON} = 5$  ms,  $\Phi = 5$  slm). When adding 10-20 ppm of NO to nitrogen, we registered  $\sim 35$ -60% reduction of initial NO content (for  $T_{ON}=1$ -5 ms) with a simultaneous production of small quantities of NO<sub>2</sub> (upper limit  $\sim 0.5$  PPM for  $T_{ON} = 5$  ms and  $\Phi = 2.5$  slm). The concentrations of N<sub>2</sub>O produced were close to those observed in the case of pure nitrogen [16].

#### *PIE*

Individual PIE waveforms of selected 1.NG, 2.PG, HIR and NO- $\gamma$  bands were registered with high statistics (accumulation of  $10^4$  samples) and with background correction. Typical corrected

emission waveforms are shown for  $T_{ON} = 1$  ms in figures 7 and 8. During the  $T_{ON}$  period, all registered emissions follow periodically the discharge current during any AC high-voltage cycle for both polarities. As soon as the discharge stops developing (during either positive or negative half-cycles), a fast drop of 1.NG emission intensity marks the beginning of the plasma layer afterglow phase (in figure 8 indicated by a vertical dash-dotted line). As evidenced in figure 8, this afterglow phase is characterised by a notably decelerated decay of the 2.PG, HIR and NO- $\gamma$  emissions. We should note here, that the position of the 2.PG (0,0) band coincides with NH( $A^3\Pi \rightarrow X^3\Sigma$ ) (0,0), NO- $\gamma$  (0,8) and NO- $\beta$  (0,9) bands at 336 nm, 337.55 nm and 337.64 nm, respectively [6,10]. The interference filter used to collect the 2.PG (0,0) band (bandwidth FWHM = 9.7 nm at 337.8 nm) could not eliminate a contribution from NH and NO emissions. The 2.PG (0,0) waveforms recorded are therefore affected, especially for later afterglow times. On the other hand, the spectral intervals used to register HIR and NO- $\gamma$  bands are free from any interfering emissions, reflecting therefore single excitation processes (pooling R3 and resonant transfer R7, respectively). Besides, we would like to mention that at longer post discharge times, we are sampling a volume that averages emissions originating both from the relaxing discharge plasma layer and from the space afterglow above it. Therefore we can focus only on the initial decay during the early post-discharge phase where the emission of the plasma layer dominates. During the early afterglow, the initial slopes of both HIR and 2.PG emissions imply an initial decay time constant  $\tau \approx 20$   $\mu$ s while NO- $\gamma$  decays with  $\tau \approx 40$   $\mu$ s, confirming that all three emissions are controlled by decaying  $N_2(A)$  species. Moreover, it was found that all initial decays are independent of either the initial NO content in the mixture or the duration  $T_{ON}$ .

### *OODR-LIF*

Contrary to the PIE waveforms, the LIF measurement gives strict insights into the space afterglow volume [13, 14]. In this case, direct OODR-LIF measurements of  $N_2(A)$  species in the space afterglow were performed at a fixed distance ( $\sim 1$  mm) from the discharge surface. The  $N_2(A)$  build-up, evolution and decay during  $T_{ON}/T_{OFF}$  periods was obtained by delaying both lasers with respect to the beginning of the  $T_{ON}$  period. For any single delay, up to 256 laser flashes were accumulated in order to improve signal-to-noise ratio. Statistically averaged OODR-LIF signals are shown in figure 9 and they clearly reveal that the  $N_2(A)$  species occur in the volume probed by the laser beams with a remarkable delay ( $\sim 2-3$  ms). After building up, the concentration of metastables remains almost unchanged throughout the  $T_{ON}$  duration and starts to decrease afterwards, confirming basically our observations made in the continuous AC regime [13]. The density of metastables increases roughly by a factor two when  $T_{ON}$  increases from 1 to 3 ms, and decreases for longer  $T_{ON}$ . During  $T_{OFF}$ , the  $N_2(A)$  from the space afterglow exhibit an approximately pure exponential decay with a single time constant on a millisecond time scale and we found a slightly increasing decay rate ( $\sim 435-1140$   $s^{-1}$ , or  $\tau \sim 2.4-0.87$

ms) when  $T_{ON}$  was increased ( $T_{ON} = 1-10$  ms). In addition, we observed that small NO admixtures (up to 60 ppm) did not change the  $N_2(A)$  decay appreciably in the space afterglow.

#### 4. Discussion

A full interpretation of experimental observations would require rather extensive numerical modelling, taking into account complex kinetic and transport phenomena. Such an analysis is however beyond the scope of this work. We will try, instead, to justify the obtained results on the basis of the most important processes which are likely responsible for the observed behaviour of  $N_2(A)$  species in the SDBD. These processes are listed in Table 1.

The relatively low energy released inside the plasma layer volume during the  $T_{ON}$  period in combination with the short duty cycle implies a very low mean power density ( $\sim 8-70$  mW/cm<sup>2</sup> for  $D = 0.048-0.33$ ). A low power density load appears to be essential in order to maintain stable discharge conditions (e.g. surface temperature of the SDBD electrode) especially for long-running OODR-LIF experiments which were performed at a minimum total gas flow  $\Phi=1$  slm.

Production of ppm levels of  $N_2O$  in nitrogen SDBD containing mainly  $O_2$  impurities can be qualitatively explained on the basis of chain reactions initiated by atomic oxygen and nitrogen. Atomic species are produced through electron impact dissociation processes during the discharge phase and R9 and R11 processes induced by metastables. Nitric monoxide produced through R11 and R20 is then converted to nitric dioxide through R17 and R18, followed by transformation to  $N_2O$  through R19. Consequently, production of  $N_2O$  species continues unless at least one of the precursors on the left hand side of R19 becomes consumed. According to [18], the R10 process should not make an important contribution due to the product branching ratio which favours R9 channel products. With sufficient densities of N atoms, a major fraction of  $O_2$  impurities should therefore be converted to  $N_2O$ . This is consistent with observations made in pure nitrogen at a high duty cycle [16]. After adding traces of NO ( $[NO] > [O_2]$ ), reactions R17, R18 and R19 should lead to a faster consumption of N atoms. Production of  $N_2O$  species through R19 then might be definitely terminated before completing  $NO_2 \rightarrow N_2O$  conversion. Such a scenario likely leads to the observed reduction of NO admixtures with simultaneous detection of  $NO_2$  and  $N_2O$  species in discharge products.

Photon-counting measurements indirectly track free electrons,  $N_2(A \Sigma_u^+)$  metastables and  $NO(X^2\Pi)$  species. Both 1.NG and 2.PG systems are easily excited by direct electron impact R1 and R2 from the  $N_2(X^1\Sigma_g^-)$  ground state. 1.NG may also be excited by electron impact from the  $N_2^+$  ground electronic state. Both emission waveforms may therefore be utilised for tracking the active discharge phase. However, an important alternative excitation source of the 2.PG emission at atmospheric pressure [6] is the energy pooling R4 between two metastable species. This is well evidenced in figures 7 and 8 showing much faster 1.NG decay with respect to 2.PG at the end of the  $T_{ON}$  period. We therefore consider the 1.NG emission waveform as the most definitive fingerprint marking extinction of SDBD

activity. The energy pooling process populates, apart from  $N_2(C^3\Pi_u)$ , the other three radiative states  $N_2(B^3\Pi_g, C^3\Pi_u, C''^5\Pi_u)$ . The great advantage of monitoring the  $N_2(C''^5\Pi_u)$  state through the HIR emission (R13) is that it always reflects the behaviour of the  $N_2(A^3\Sigma_u^+)$  species. This is because under the inspected conditions, the  $N_2(C''^5\Pi_u)$  state is populated by the energy pooling R3 process exclusively [6, 9, 10]. Concerning the NO- $\gamma$  bands, the NO( $A^2\Sigma^+$ ) electronic state is produced through the well-known resonant energy transfer process R7 followed by R16 and monitors indirectly the behaviour of the  $N_2(A)$  metastable in the discharge layer, as well as in the space afterglow if the NO density is almost constant. The observed decay rates of HIR and NO- $\gamma$  emissions at the beginning of the  $T_{OFF}$  period imply that the  $N_2(A^3\Sigma_u^+)$  species are quickly quenched with a characteristic initial loss rate of about  $2.5 \times 10^4 \text{ s}^{-1}$  ( $\tau \approx 40 \text{ }\mu\text{s}$ ). Such a loss rate cannot be due to R7 or R9 because it would require significant quencher densities  $[\text{NO}] \sim 4 \times 10^{14} \text{ cm}^{-3}$  or  $[\text{O}_2] \sim 1 \times 10^{16} \text{ cm}^{-3}$ . Oxygen impurities remain below 3 ppm ( $[\text{O}_2] < 7.5 \times 10^{13} \text{ cm}^{-3}$ ) indicating a maximum loss rate of about  $180 \text{ s}^{-1}$ . Even after assuming instantaneous and complete conversion of  $\text{O}_2$  impurities to nitric oxide ( $[\text{NO}] < 1.5 \times 10^{14} \text{ cm}^{-3}$ ), this would still provide an insufficient loss rate of about  $5 \times 10^3 \text{ s}^{-1}$ . Other potential quenchers are  $N_2(X^1\Sigma^+, v=0)$ ,  $N_2(X^1\Sigma^+, v \geq 5)$  and  $N(^4S)$  species through R5, R6 and R8, respectively. The recommended rate of R5 [18] implies negligible quenching with a loss rate of about  $65 \text{ s}^{-1}$ . Reactions R6 and R8 have very similar rate constants and the density ( $[\text{N}^4S] + [\text{N}_2(X^1\Sigma^+, v \geq 5)]$ )  $\sim 5 \times 10^{14} \text{ cm}^{-3}$  would be sufficient to provide the required loss rate. However, such a density of highly vibrationally excited molecules would require a vibrational temperature of about 1500 K and production of both  $N_2(X^1\Sigma^+, v \geq 5)$  and  $N(^4S)$  species should tend to be enhanced with increasing  $T_{ON}$ . Nitrogen atom densities of up to  $5 \times 10^{14} \text{ cm}^{-3}$  were in fact reported in continuously excited atmospheric volume DBD and corona discharges in pure nitrogen [20–22]. However, it has been clearly shown that such  $[\text{N}^4S]$  densities occur both in the Townsend and filamentary DBD regimes due to inefficient removal of nitrogen atoms through  $\text{N}+\text{N}+\text{M}$  recombination, which leads to accumulation of atomic species produced during successive discharge cycles. By means of the calibrated TALIF technique [22], nitrogen atom densities  $\sim 2 \times 10^{14} \text{ cm}^{-3}$  were fixed at a mean energy density dissipated in the gas  $\geq 10 \text{ mJ/cm}^3$  while showing a clearly decreasing trend at lower energy densities. Estimating the thickness of the SDBD plasma layer  $\sim 10^{-2} - 10^{-3} \text{ cm}$ , we can evaluate the mean energy density dissipated during the  $T_{ON}$  period to be  $\sim 0.1 - 1 \text{ mJ/cm}^3$  (for  $T_{ON} = 3 \text{ ms}$ ). In addition, all nitrogen atoms are produced close to the SDBD electrode surface which provides, compared to volume DBD, a much more efficient third body for their recombination. Therefore, N atom densities produced in amplitude modulated AC surface DBD at the investigated duty cycles should be significantly below the values reported in [22]. Finally, the experimentally observed independence of initial loss rate of metastables on both NO admixtures and  $T_{ON}$  duration allows to discard  $\text{O}_2$  impurities and their related conversion products

( $N_xO_y$ ) as well as  $N_2(X^1\Sigma^+, v \geq 5)$  and  $N(^4S)$  species, as the dominant quenchers of metastables at the beginning of the  $T_{OFF}$  period. It is therefore very likely that the fast loss rate of metastables at the end of the  $T_{ON}$  period is mainly caused by self-quenching through pooling as in the case of volume corona discharges [9, 15]. Decay of metastables caused exclusively by pooling processes R3 and R4 at the experimentally observed loss rate would require average metastable densities  $[N_2(A^3\Sigma_u^+)] \sim 2 \times 10^{13} \text{ cm}^{-3}$ . Fixing the early afterglow metastable density at  $[N_2(A^3\Sigma_u^+)] \sim 2 \times 10^{13} \text{ cm}^{-3}$  would imply a maximum average metastable density during  $T_{ON}$  of  $[N_2(A^3\Sigma_u^+)] \sim 9 \times 10^{13} \text{ cm}^{-3}$  (estimated through the relative intensity of HIR emission). However, due to the SDBD electrode geometry, micro-discharge filaments are produced very close to the dielectric surface and filament roots are even in direct contact with metallic stripes. Quenching of metastables on the electrode surface therefore must be seriously considered.

The delayed build-up of  $N_2(A)$  observed through OODR-LIF in the space afterglow evidences diffusion as a primary process responsible for transportation of metastables from the site of production (micro-discharge filaments occurring close to the discharge electrode surface) to the point of observation in the space afterglow. The variable decay time of  $N_2(A)$  ( $\tau \sim 2.4\text{--}0.87 \text{ ms}$  for  $T_{ON} = 1\text{--}10 \text{ ms}$ ) implying a loss rate of  $\sim 417\text{--}1150 \text{ s}^{-1}$ ) evidences relaxation controlled by diffusion with some gas-phase collisional loss. The build-up time, measured during  $T_{ON}$ , indicates that the characteristic diffusion time is  $\sim 3 \text{ ms}$  with a corresponding loss rate  $\sim 330 \text{ s}^{-1}$ . Attributing again all the initial loss rate  $\sim 417 \text{ s}^{-1}$  ( $\tau \sim 2.4 \text{ ms}$  for  $T_{ON} = 1 \text{ ms}$ ) to self-quenching through pooling would require an upper limit for metastable density in the space afterglow of  $[N_2(A^3\Sigma_u^+)] \sim 1 \times 10^{12} \text{ cm}^{-3}$ . Considering enhanced production of  $N_xO_y$  as well as  $N_2(X^1\Sigma^+, v \geq 5)$  and  $N(^4S)$  species when increasing  $T_{ON}$ , the difference between minimum (for  $T_{ON} = 1 \text{ ms}$ ) and maximum (for  $T_{ON} = 10 \text{ ms}$ ) loss rates  $\sim 730 \text{ s}^{-1}$  should be attributed to these quenchers. On the other hand, the density  $[N_2(A^3\Sigma_u^+)] \sim 10^{11} \text{ cm}^{-3}$  estimated for the continuous AC regime [13] should be taken here as a lower limit, since in the continuous AC regime the maximum concentration of  $N_2(A)$  quenchers is produced.

## 5. Conclusions

The behaviour of  $N_2(A^3\Sigma_u^+)$  metastable species produced by SDBD driven in the amplitude-modulated AC regime was revealed both in a thin surface plasma layer and in the space afterglow. Basically, the  $N_2(A^3\Sigma_u^+)$  species in the plasma layer observed through HIR emission follow the discharge current oscillations. During the early afterglow, both HIR and 2.PG emissions decay exponentially with  $\tau \sim 20 \text{ ms}$  while  $NO\text{--}\gamma$  decays with  $\tau \sim 40 \text{ ms}$ , all independently of either initial  $NO$  concentration or  $T_{ON}$  length. This evidences that all three emissions are controlled by  $N_2(A)$  species. Additionally, assuming pooling as an exclusive loss channel allows a rough estimation of the average metastable density produced in a thin surface plasma layer of  $[N_2(A^3\Sigma_u^+)] \sim 9 \times 10^{13} \text{ cm}^{-3}$ .

Metastables observed through the OODR-LIF signal in the space afterglow build up after a delay ( $\sim 2$  ms), remain almost unchanged for the duration of  $T_{ON}$  and decay exponentially afterwards with a millisecond time scale  $\tau \sim 0.87\text{--}2.4$  ms. Evolution of the OODR-LIF signal clearly evidences that in the SDBD a stable cloud of  $N_2(A)$  metastables is formed mainly by diffusion. The density of metastables occurring in the space afterglow (1 mm from the electrode surface) can be reasonably estimated to be in the range  $10^{11} \leq [N_2(A^3\Sigma_u^+)] \leq 10^{12}$   $\text{cm}^{-3}$ .

Further experiments are however necessary in order to (i) evaluate the contribution of surface processes to initial  $N_2(A)$  quenching rate and (ii) to better understand the behavior of produced/admixed nitric oxide in the space afterglow for calibrating the OODR-LIF signal reliably. To this end, side-on emission spectrometry performed with higher spatial resolution on a single micro-discharge might help to fix the metastable densities in both plasma and space afterglow layers with much higher confidence. Preparation of such experiments is in progress.

### **Acknowledgments**

Joint investigation performed in the framework of CNR - AV ČR cooperative agreement No. 132.02.1 (A.A. 2007-2009). IPP Prague's experiments supported by the GAČR under contract No. 202/08/1106.

Table 1. Processes influencing N<sub>2</sub>(A) state evolution in atmospheric-pressure SDBD driven in pure nitrogen and in nitrogen containing NO traces.

	Process <sup>§</sup>	Rate coefficient	Ref.
R1	N <sub>2</sub> + e → N <sub>2</sub> (A <sup>3</sup> Σ <sub>u</sub> <sup>+</sup> , B <sup>3</sup> Π <sub>g</sub> , C <sup>3</sup> Π <sub>u</sub> , ...) + e	k=k(T <sub>e</sub> )	[-]
R2	N <sub>2</sub> + e → N <sub>2</sub> <sup>+</sup> (X <sup>2</sup> Σ <sub>g</sub> <sup>+</sup> , B <sup>2</sup> Σ <sub>u</sub> <sup>+</sup> , ...) + e + e'	k=k(T <sub>e</sub> )	[-]
R3	N <sub>2</sub> (A <sup>3</sup> Σ <sub>u</sub> <sup>+</sup> ) + N <sub>2</sub> (A <sup>3</sup> Σ <sub>u</sub> <sup>+</sup> ) → N <sub>2</sub> + N <sub>2</sub> (C'' <sup>5</sup> Π <sub>u</sub> )	k = (8.1-9.9) x 10 <sup>-11</sup> [cm <sup>3</sup> s <sup>-1</sup> ]	[9]
R4	N <sub>2</sub> (A <sup>3</sup> Σ <sub>u</sub> <sup>+</sup> ) + N <sub>2</sub> (A <sup>3</sup> Σ <sub>u</sub> <sup>+</sup> ) → N <sub>2</sub> + N <sub>2</sub> (C <sup>3</sup> Π <sub>u</sub> )	k = 1.5 x 10 <sup>-10</sup> [cm <sup>3</sup> s <sup>-1</sup> ]	[9]
R5	N <sub>2</sub> (A <sup>3</sup> Σ <sub>u</sub> <sup>+</sup> ) + N <sub>2</sub> (X <sup>1</sup> Σ <sup>+</sup> ) → N <sub>2</sub> * + N <sub>2</sub> (X <sup>1</sup> Σ <sup>+</sup> )	k = (2.6-370) x 10 <sup>-18</sup> [cm <sup>3</sup> s <sup>-1</sup> ]	[18]
R6	N <sub>2</sub> (A <sup>3</sup> Σ <sub>u</sub> <sup>+</sup> ) + N <sub>2</sub> (X <sup>1</sup> Σ <sup>+</sup> , v≥5) → N <sub>2</sub> (B <sup>3</sup> Π <sub>g</sub> ) + N <sub>2</sub>	k = 3 x 10 <sup>-11</sup> [cm <sup>3</sup> s <sup>-1</sup> ]	[9]
R7	N <sub>2</sub> (A <sup>3</sup> Σ <sub>u</sub> <sup>+</sup> ) + NO(X <sup>2</sup> Π) → N <sub>2</sub> + NO(A <sup>2</sup> Σ <sup>+</sup> )	k = (6.5-11) x 10 <sup>-11</sup> [cm <sup>3</sup> s <sup>-1</sup> ]	[17]
R8	N <sub>2</sub> (A <sup>3</sup> Σ <sub>u</sub> <sup>+</sup> ) + N( <sup>4</sup> S) → N <sub>2</sub> + N( <sup>2</sup> P)	k = 5 x 10 <sup>-11</sup> [cm <sup>3</sup> s <sup>-1</sup> ]	[9]
R9	N <sub>2</sub> (A <sup>3</sup> Σ <sub>u</sub> <sup>+</sup> ) + O <sub>2</sub> (X <sup>3</sup> Σ <sub>g</sub> <sup>+</sup> ) → N <sub>2</sub> + 2O( <sup>3</sup> P, <sup>1</sup> D), O <sub>2</sub> *	k = (2.4-5.5) x 10 <sup>-12</sup> [cm <sup>3</sup> s <sup>-1</sup> ]	[17]
R10	N <sub>2</sub> (A <sup>3</sup> Σ <sub>u</sub> <sup>+</sup> ) + O <sub>2</sub> (X <sup>3</sup> Σ <sub>g</sub> <sup>+</sup> ) → N <sub>2</sub> O + O	<i>see discussion in ref.[18]</i>	[18]
R11	N <sub>2</sub> (A <sup>3</sup> Σ <sub>u</sub> <sup>+</sup> ) + O( <sup>3</sup> P) → NO + N( <sup>4</sup> S, <sup>2</sup> D)	k = (3-5.2) x 10 <sup>-12</sup> [cm <sup>3</sup> s <sup>-1</sup> ]	[17]
R12	N <sub>2</sub> (A <sup>3</sup> Σ <sub>u</sub> <sup>+</sup> ) → N <sub>2</sub> (X <sup>1</sup> Σ <sub>g</sub> <sup>+</sup> ) + hv <sub>VK</sub>	ν = (4.7-4.9) x 10 <sup>-1</sup> [s <sup>-1</sup> ]	[9]
R13	N <sub>2</sub> (C'' <sup>5</sup> Π <sub>u</sub> ) → N <sub>2</sub> (A <sup>5</sup> Σ <sub>g</sub> <sup>+</sup> ) + hv <sub>HIR</sub>	ν ~ 2.3 x 10 <sup>5</sup> /2.5 x 10 <sup>7</sup> [s <sup>-1</sup> ]	[9]
R14	N <sub>2</sub> (C <sup>3</sup> Π <sub>u</sub> ) → N <sub>2</sub> (B <sup>3</sup> Π <sub>g</sub> ) + hv <sub>2.PG</sub>	ν = (2.4-2.7) x 10 <sup>7</sup> [s <sup>-1</sup> ]	[9]
R15	N <sub>2</sub> (B <sup>3</sup> Π <sub>g</sub> ) → N <sub>2</sub> (A <sup>3</sup> Σ <sub>u</sub> <sup>+</sup> ) + hv <sub>1.PG</sub>	ν = (0.8-2.5) x 10 <sup>5</sup> [s <sup>-1</sup> ]	[9]
R16	NO(A <sup>2</sup> Σ <sup>+</sup> ) → NO(X <sup>2</sup> Π) + hv <sub>γ</sub>	ν = 4.9 x 10 <sup>6</sup> [s <sup>-1</sup> ]	[9]
R17	NO + N( <sup>4</sup> S) → N <sub>2</sub> + O( <sup>3</sup> P)	k = 3 x 10 <sup>-11</sup> [cm <sup>3</sup> s <sup>-1</sup> ]	[19]
R18	NO + O( <sup>3</sup> P) + N <sub>2</sub> → NO <sub>2</sub> + N <sub>2</sub>	k = 2.1 x 10 <sup>-12</sup> [cm <sup>3</sup> s <sup>-1</sup> ]	[19]
R19	NO <sub>2</sub> + N( <sup>4</sup> S) → N <sub>2</sub> O + O( <sup>3</sup> P)	k = 1.2 x 10 <sup>-11</sup> [cm <sup>3</sup> s <sup>-1</sup> ]	[19]
R20	O( <sup>3</sup> P) + N( <sup>4</sup> S) + N <sub>2</sub> → NO(A <sup>2</sup> Σ <sup>+</sup> , B <sup>2</sup> Π, C <sup>2</sup> Π) + N <sub>2</sub>	k = 1 x 10 <sup>-32</sup> [cm <sup>6</sup> s <sup>-1</sup> ]	[9]

<sup>§</sup> N<sub>2</sub> ≡ N<sub>2</sub>(X<sup>1</sup>Σ<sup>+</sup>), NO ≡ NO(X<sup>2</sup>Π)

## References

- [1] Masuda S, Akutsu K, Kuroda M, Awatsu Y and Shibuya Y 1988 A ceramic-based ozonizer using high-frequency discharge *IEEE Trans. Ind. Appl.* **24** 223-31
- [2] Oda T, Yamashita R, Haga I, Takahashi T and Masuda S 1996 Decomposition of gaseous organic contaminants by surface discharge induced plasma chemical processing SPCP *IEEE Trans. Ind. Appl.* **32** 118-24
- [3] Ráhel' J, Šimor M, Černák M, Štefečka M, Imahori Y and Kando M 2003 Hydrophilization of polypropylene nonwoven fabric using surface barrier discharge *Surface and Coating Technol.* **169-170** 604-08
- [4] Engemann J and Korzec D 2003 Assessment of discharges for large area atmospheric pressure plasma-enhanced chemical vapor deposition (AP PE-CVD) *Thin Solid Films* **442** 36-39
- [5] Massines F, Ségur P, Gherardi N, Khamphan C and Ricard A 2003 Physics and chemistry in a glow dielectric barrier discharge at atmospheric pressure: diagnostics and modeling *Surface and Coatings Technology* **174-175** 8-14
- [6] Šimek M, Babický V, Člupek M, and Šunka P 2001 Observation of N<sub>2</sub> Herman Infrared system in pulsed positive streamer induced emission at atmospheric pressure *J.Phys.D:Appl.Phys.* **34** 3185-90
- [7] Šimek M 2002 The modelling of streamer-induced emission in atmospheric pressure, pulsed positive corona discharge: N<sub>2</sub> Second Positive and NO-γ systems *J.Phys.D:Appl.Phys.* **35** 1967-80
- [8] Šimek M, DeBenedictis S, Dilecce G, Babický V, Člupek M, and Šunka P 2002 Time and space resolved analysis of N<sub>2</sub>(C<sup>3</sup>Π<sub>u</sub>) vibrational distributions in pulsed positive corona discharge *J.Phys.D:Appl.Phys.* **35** 1981-90
- [9] Šimek M 2003 Determination of N<sub>2</sub>(A<sup>3</sup>Σ<sup>+</sup>) metastable density produced by nitrogen streamers at atmospheric pressure: 1. Design of diagnostic method *Plasma Sources Sci. Technol.* **12**, 421-431
- [10] Šimek M 2003 Determination of N<sub>2</sub>(A<sup>3</sup>Σ<sup>+</sup>) metastable density produced by nitrogen streamers at atmospheric pressure: 2. Experimental verification *Plasma Sources Sci. Technol.* **12**, 454-463
- [11] Šimek M, Člupek M, Babický V and Šunka P 2006 Production of reactive species by atmospheric pressure streamers in N<sub>2</sub>-O<sub>2</sub> mixtures, *Pure Appl. Chem.* **6** 1213–1225
- [12] Dilecce G, Ambrico P F and DeBenedictis S 2007 N<sub>2</sub>(A<sup>3</sup>Σ<sup>+</sup>) density measurement in a dielectric barrier discharge in N<sub>2</sub> and N<sub>2</sub> with small O<sub>2</sub> admixtures *Plasma Sources Sci. Technol.* **16** 511-522
- [13] Ambrico P F, Šimek M, Dilecce G and De Benedictis S 2008 On the Measurement of

- $N_2(A^3\Sigma_u^+)$  Metastable in  $N_2$  Surface-Dielectric Barrier Discharge at Atmospheric Pressure  
*Plasma Chem. Plasma Process.* **28** 299-316
- [14] Ambrico P F, Šimek M, Dilecce G and De Benedictis S 2009  $N_2(A^3\Sigma_u^+)$  time evolution in  $N_2$  atmospheric pressure surface dielectric barrier discharge driven by ac voltage under modulated regime *Appl. Phys. Letters* **94** 231503
- [15] Ono R, Tobaru C, Teramoto Y and Oda T 2009 Laser-induced fluorescence of  $N_2(A^3\Sigma^+)$  metastable in  $N_2$  pulsed positive corona discharge  
*Plasma Sources Sci. Technol.* **18** 025006
- [16] Šimek M and Prukner V 20xx NO reduction efficiency by  $N_2$  surface dielectric barrier discharge under modulated AC regime (to be published)
- [17] Golde M F 1988 Reactions of  $N_2(A^3\Sigma_u^+)$  *Int.J.Chem.Kinet.* **20** 75-92
- [18] Herron J T 1999 Evaluated Chemical Kinetics Data for Reactions of  $N(^2D)$ ,  $N(^2P)$  and  $N_2(A^3\Sigma_u^+)$  in the Gas Phase *J.Phys.Chem.Ref.Data* **28** 1453-92
- [19] Herron J T and Green D S 2000 Chemical Kinetics Database and Predictive Schemes for Nonthermal Humid Air Plasma Chemistry. Part II. Neutral Species Reactions  
*Plasma Chem. Plasma Process.* **21** 459-81
- [20] Fromy P, Pointu A M, Ganciu M, and Orphal J 2006 Transportation of nitrogen atoms in an atmospheric pressure post-discharge of pure nitrogen *J. Phys.D: Appl.Phys* **39** 108-112
- [21] Oinuma G, Inanaga Y, Noda S, Tanimura Y, Kuzumoto M, Tabata Y, and Watanabe K 2008 Method for real-time measurement of nitrogen atom density in atmospheric pressure post-discharge flows *J. Phys.D: Appl.Phys* **41** 155204
- [22] Es-Sebbar E, Sarra-Bournet C, Naudé N, Massines F and Gherardi N 2009 Absolute nitrogen atom density measurements by two-photon laser-induced fluorescence spectroscopy in atmospheric pressure dielectric barrier discharges of pure nitrogen  
*J. Appl. Phys.* **106** 073302

## Figure captions

- Figure 1.** Schematic diagram of the experimental set-up.
- Figure 2.** Sketch of the SDBD reactor with PIE observation and OODR-LIF excitation-detection geometries.
- Figure 3.** Energy levels involved in monitoring  $N_2(A)$  through PIE and OODR-LIF techniques.
- Figure 4.** Photograph of the discharge in pure nitrogen ( $\Phi = 2,5$  slm,  $T_{ON} = 1$  ms).
- Figure 5.** Typical electrical and optical characteristics of the discharge in pure nitrogen ( $\Phi = 5$  slm,  $T_{ON} = 1$  ms).
- Figure 6.** Typical Lissajous characteristics of the discharge in pure nitrogen ( $\Phi = 5$  slm,  $T_{ON} = 1$  ms).
- Figure 7.** Typical 1.NG, 2.PG, HIR and NO- $\gamma$  emission waveforms observed in pure nitrogen ( $\Phi = 5$  slm,  $T_{ON} = 1$  ms).
- Figure 8.** Initial decays of 1.NG, 2.PG, HIR and NO- $\gamma$  emission waveforms observed in pure nitrogen ( $\Phi = 5$  slm,  $T_{ON} = 1$  ms). Dotted lines indicate characteristic decay rates of emitting species.
- Figure 9.** Build-up and decay of the OODR-LIF signal in the space afterglow at 1 mm for  $T_{ON} = 1,3,5$  and 10 ms and  $T_{OFF} = 20$  ms (pure nitrogen,  $\Phi = 1$  slm).

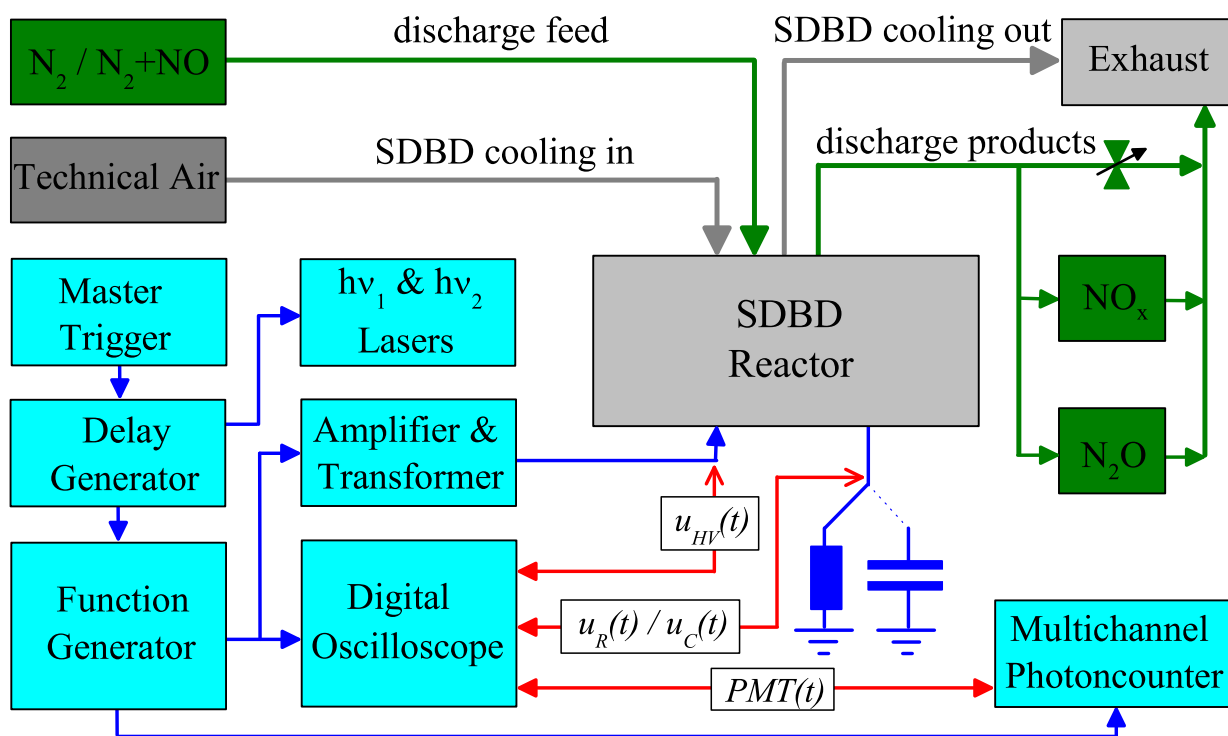


Figure 1 (figure\_1.EPS)

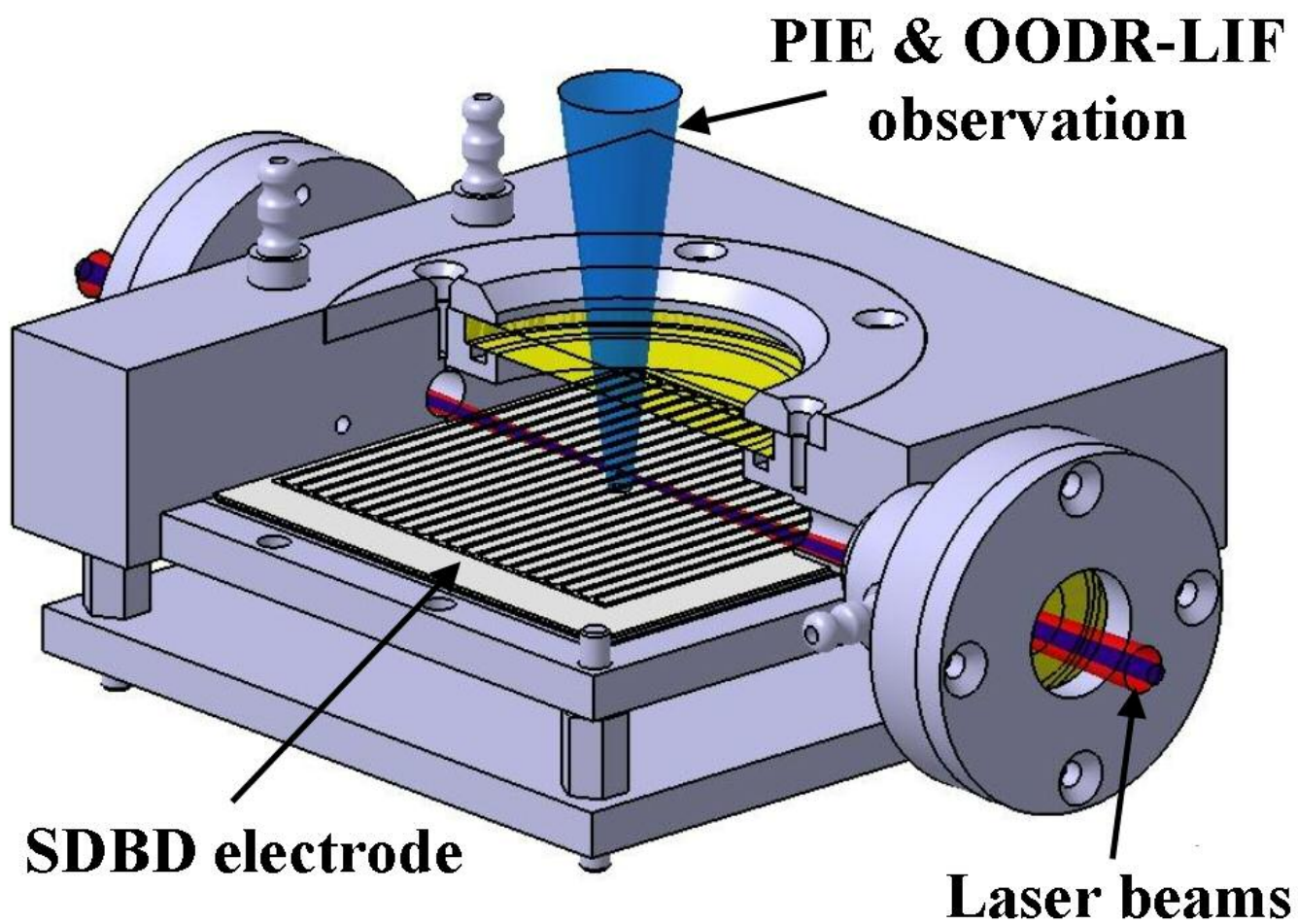


Figure 2 (figure\_2.tif)

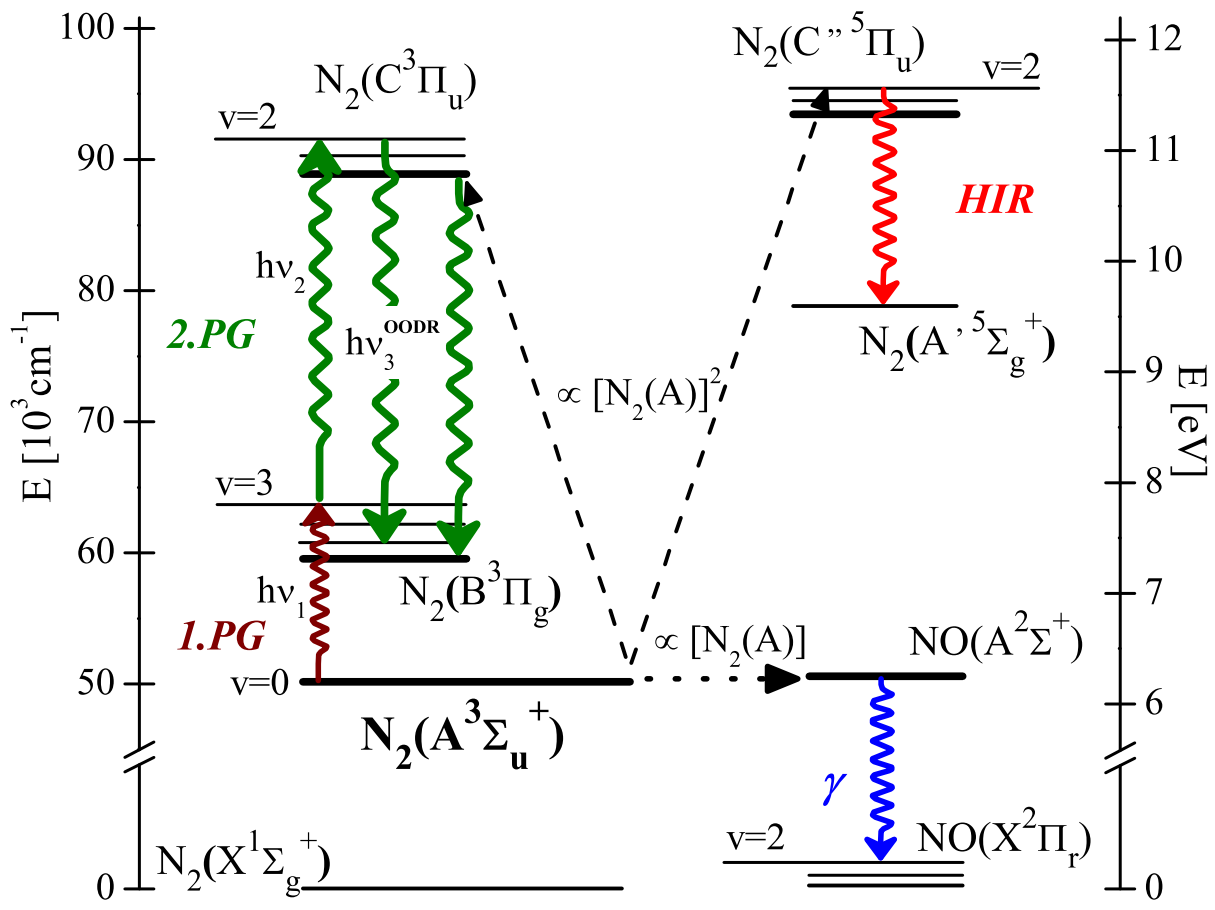


Figure 3 (figure\_3.EPS)

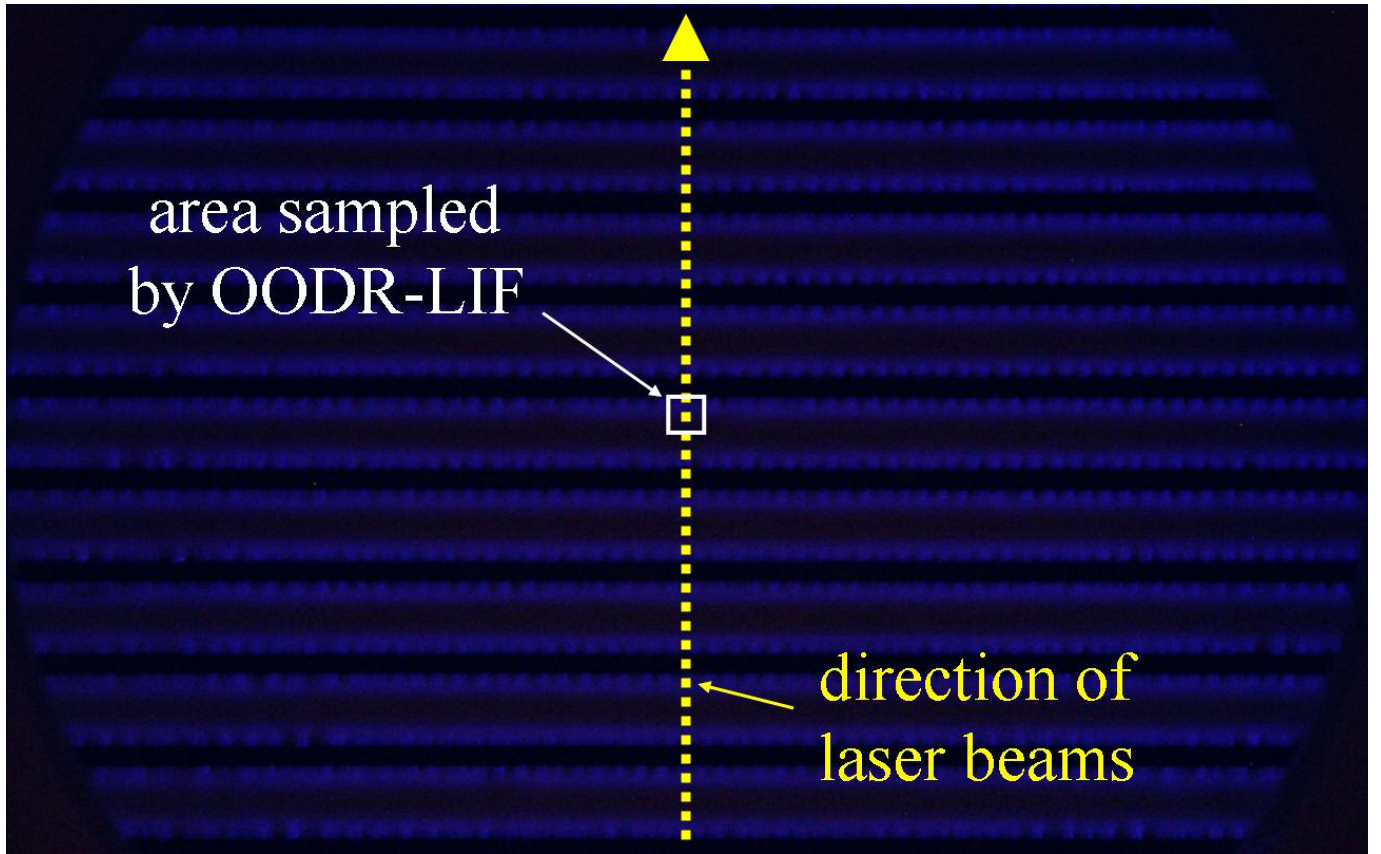


Figure 4 (figure\_4.tif)

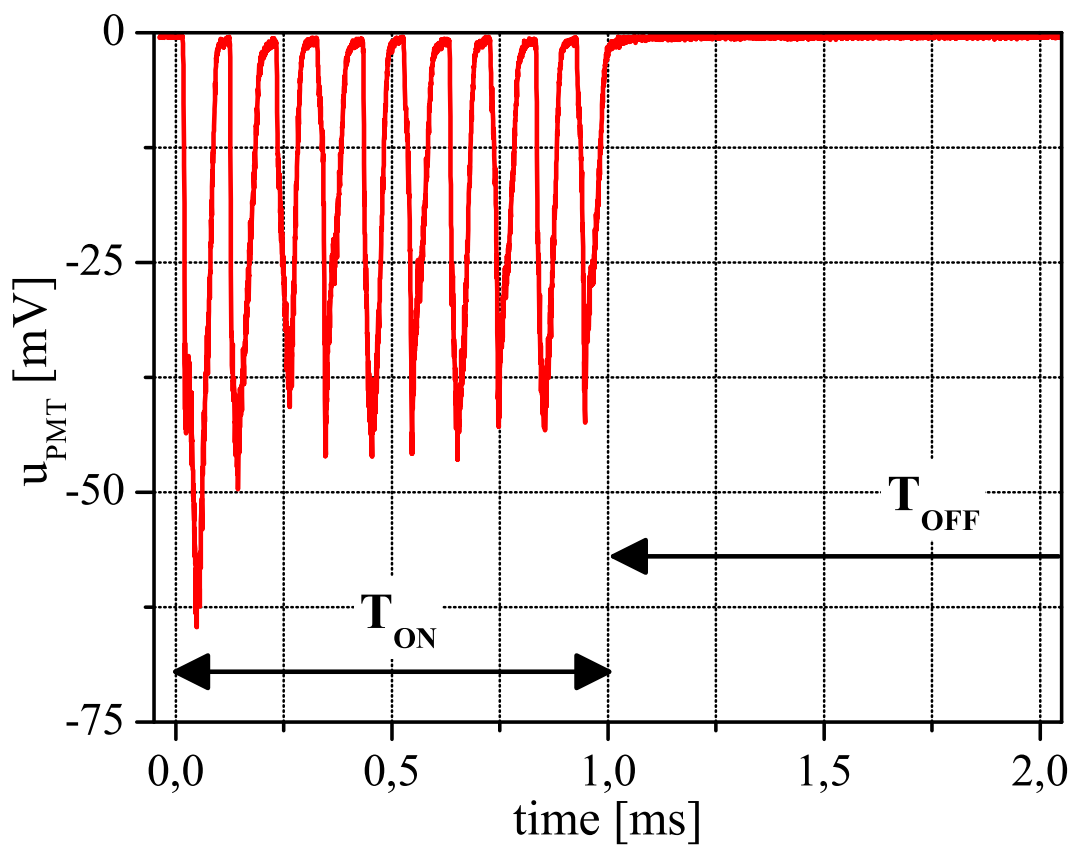
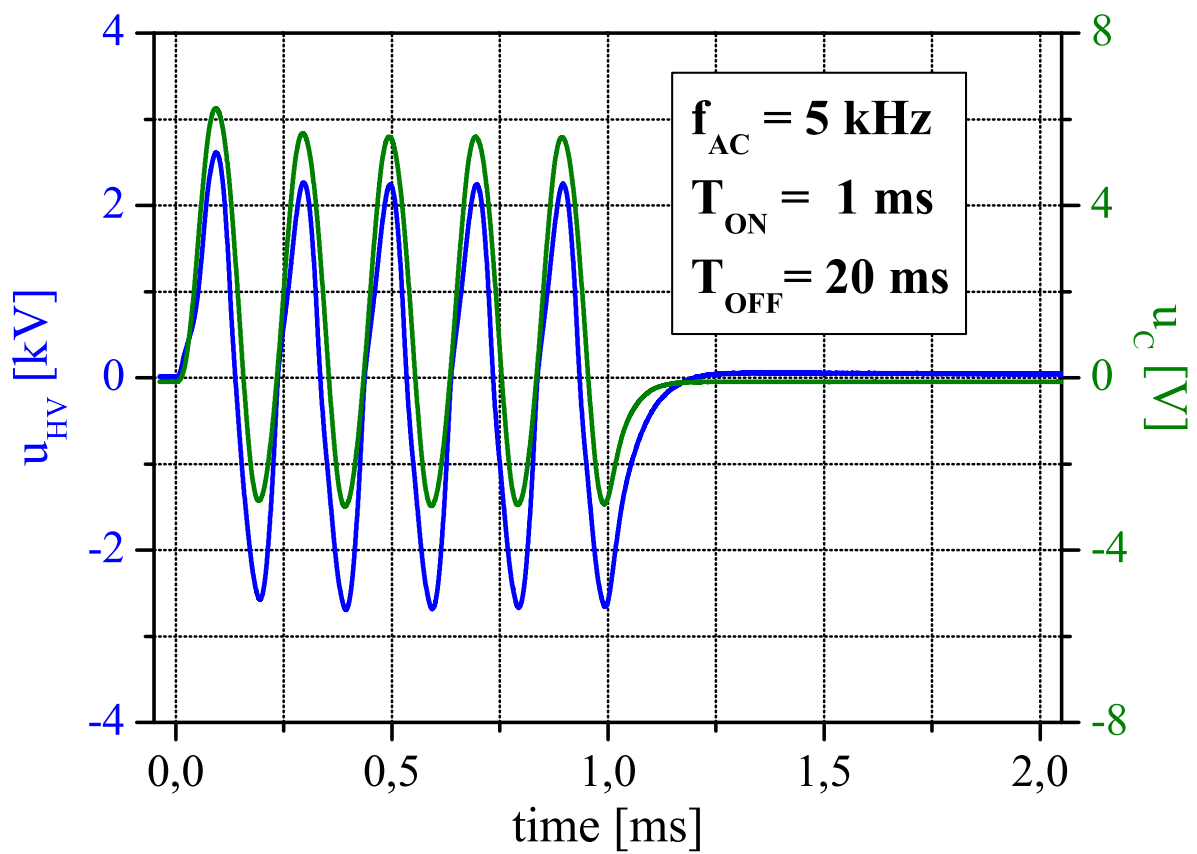


Figure 5 (figure\_5.EPS)

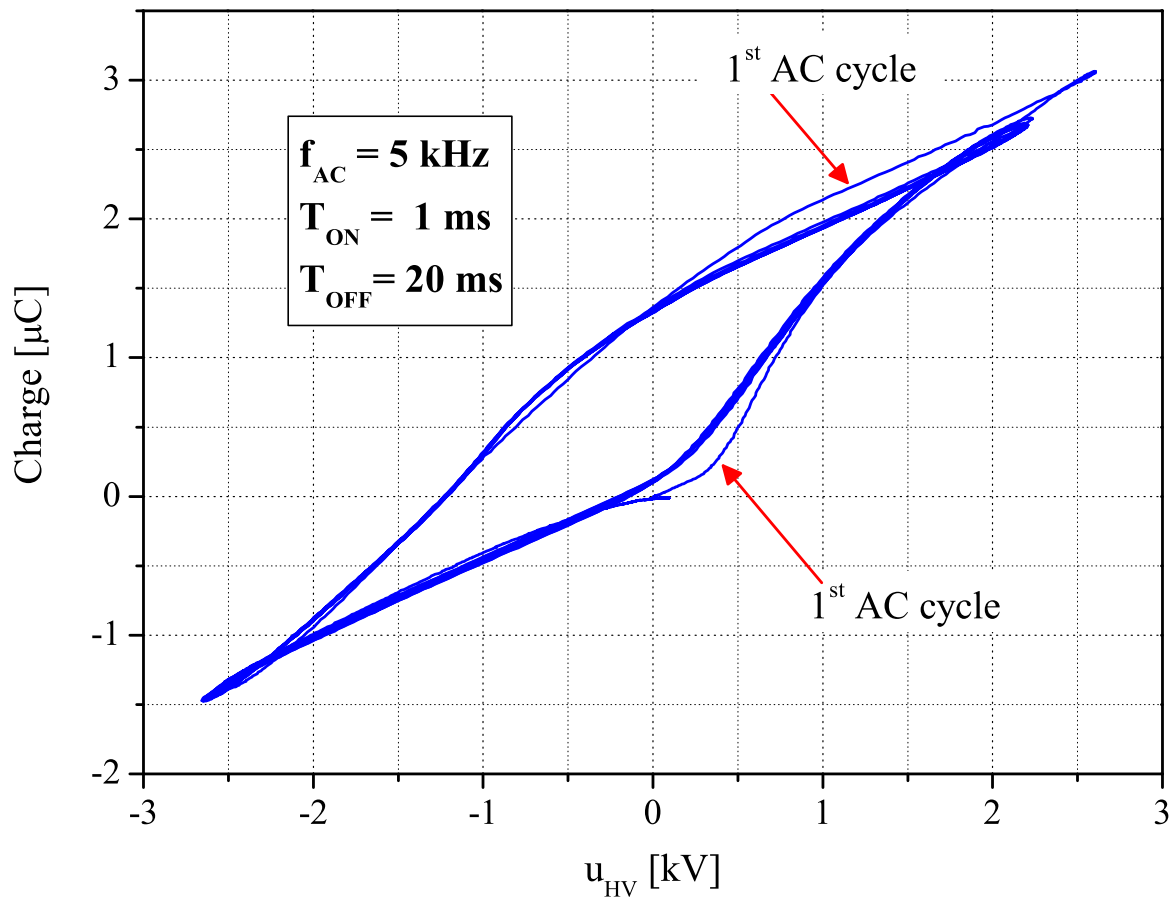


Figure 6 (figure\_6\_revised.EPS)

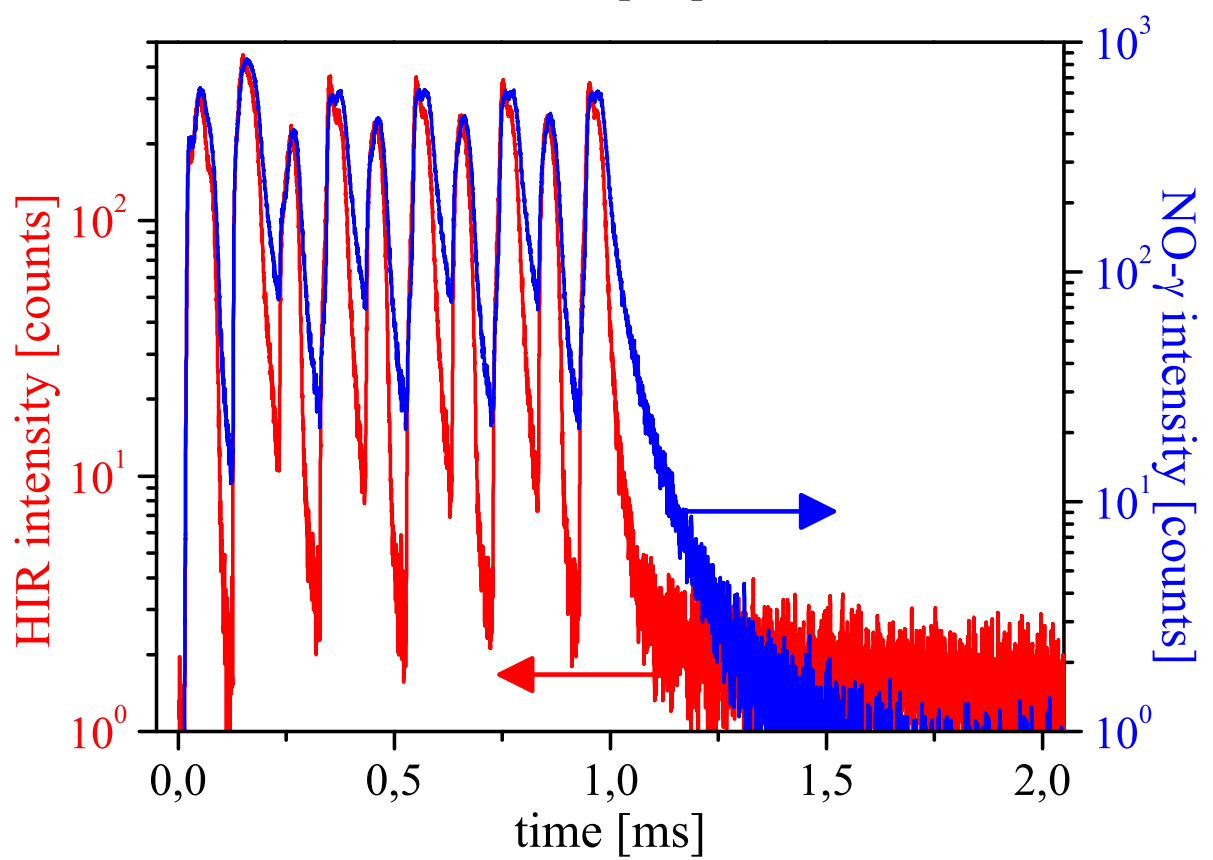
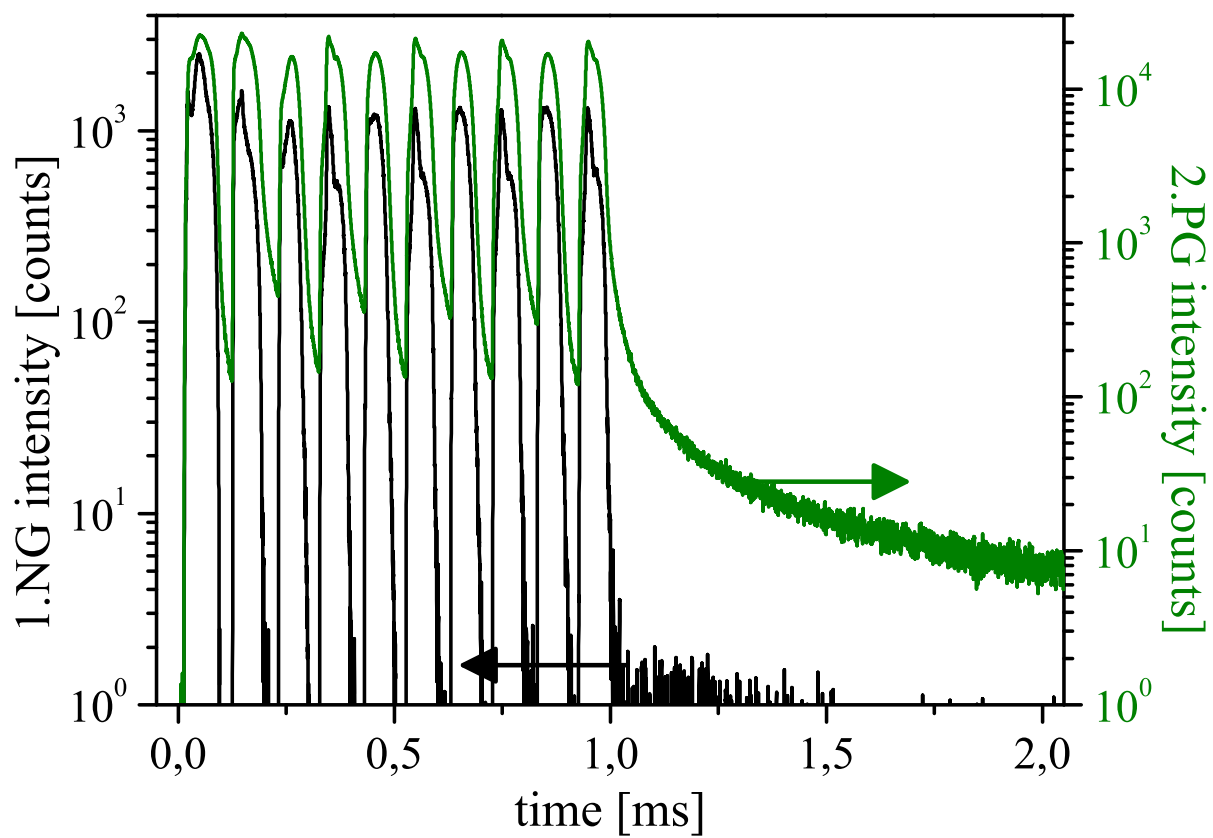


Figure 7 (figure\_7.EPS)

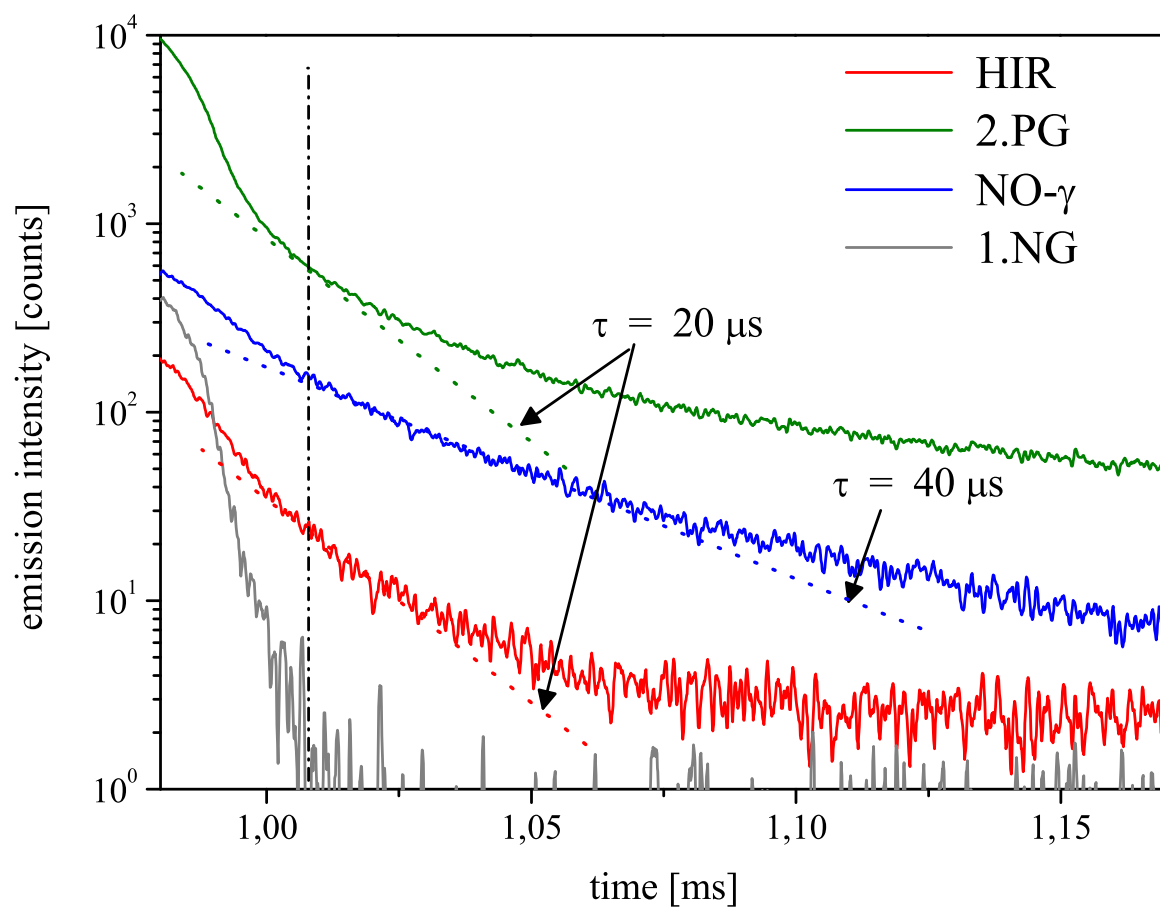


Figure 8 (figure\_8.EPS)

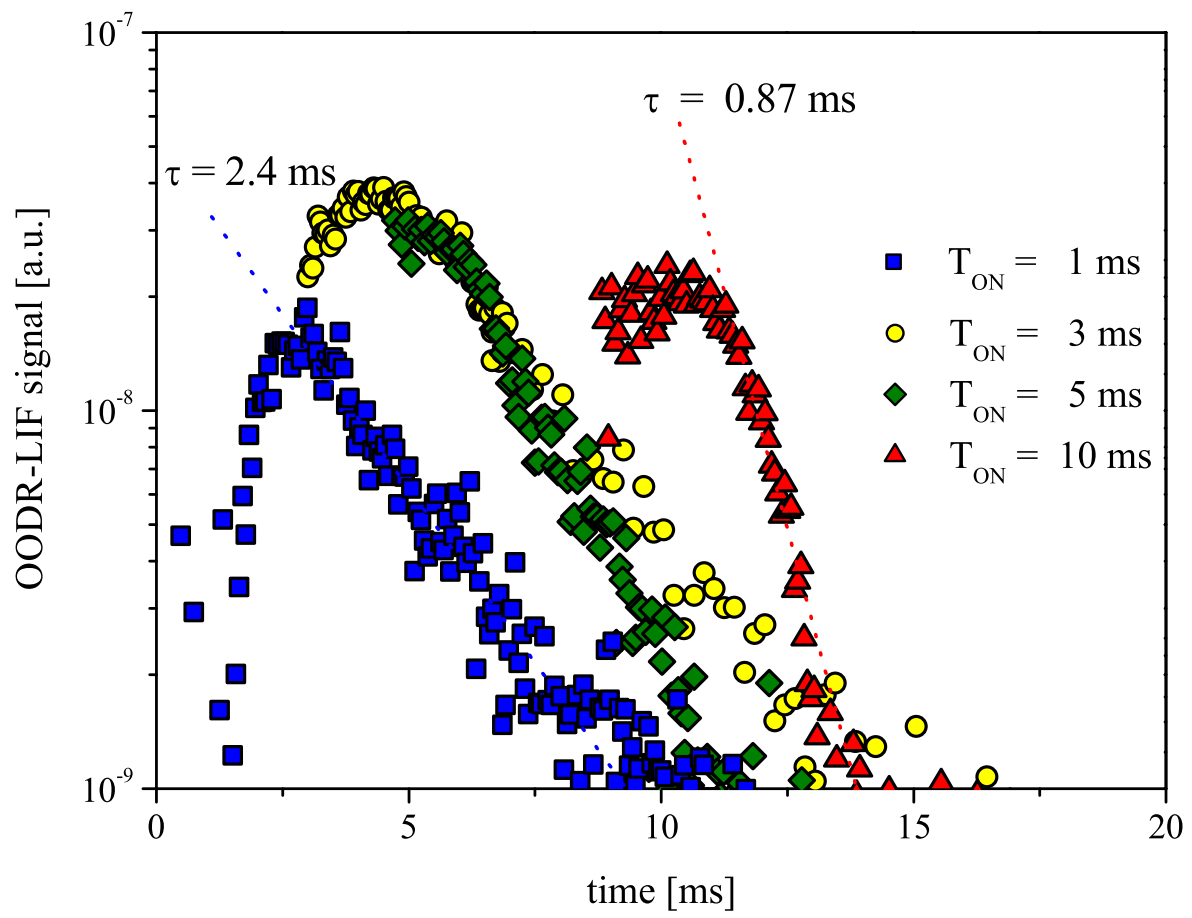


Figure 9 (figure\_9.EPS)